Annals of Nuclear Energy 85 (2015) 763–775

Contents lists available at ScienceDirect

Annals of Nuclear Energy

journal homepage: www.elsevier.com/locate/anucene

Neutronics and fuel performance evaluation of accident tolerant FeCrAl cladding under normal operation conditions

Xu Wu [a,*], Tomasz Kozlowski [a], Jason D. Hales [b]

[a] Department of Nuclear, Plasma and Radiological Engineering, University of Illinois at Urbana-Champaign, 124 Talbot Laboratory, 104 South Wright Street, Urbana, IL 61801, USA
[b] Fuels Modeling & Simulation Department, Idaho National Laboratory, Idaho Falls, ID 83415, USA

ARTICLE INFO

Article history:
Received 6 May 2015
Received in revised form 11 June 2015
Accepted 17 June 2015
Available online 29 June 2015

Keywords:
FeCrAl
Accident Tolerant Fuel

ABSTRACT

Neutronics and fuel performance analysis is done for enhanced accident tolerance fuel (ATF), with the Monte Carlo reactor physics code Serpent and INL's fuel performance code BISON. The purpose is to evaluate the most promising ATF candidate material FeCrAl, which has excellent oxidation resistance, as fuel cladding under normal operational conditions.

Due to several major disadvantages of FeCrAl coating, such as difficulty in fabrication, diametrical compression from reactor pressurization, coating spallation and inter diffusion with zirconium, a monolithic FeCrAl cladding design is suggested. To overcome the neutron penalty expected when using FeCrAl as cladding for current oxide fuel, an optimized FeCrAl cladding design from a detailed parametric study in literature is adopted, which suggests reducing the cladding thickness and slightly increasing the fuel enrichment. A neutronics analysis is done that implementing this FeCrAl cladding design in a Pressurized Water Reactor (PWR) single assembly. The results show that the PWR cycle length requirements will be matched, with a slight increase in total plutonium production.

Fuel performance analysis with BISON code is carried out to investigate the effects with this FeCrAl cladding design. The results demonstrate that the application of FeCrAl cladding could improve performance. For example, the axial temperature profile is flattened. The gap closure is significantly delayed, which means the pellet cladding mechanical interaction is greatly delayed. The disadvantages for monolithic FeCrAl cladding are that: (1) fission gas release is increased; and (2) fuel temperature is increased, but the increase is less than 50 K even at high burnup.

The better strength, corrosion, and embrittlement properties of FeCrAl enable the fabrication of FeCrAl cladding with thinner walls. FeCrAl cladding proves to be a good alternate for zircaloy cladding, given the advantages and insignificant disadvantages shown by fuel performance analysis.

© 2015 Elsevier Ltd. All rights reserved.

1. Introduction

Following the Fukushima Daiichi nuclear disaster in 2011, the emphasis for nuclear fuel R&D activities has shifted from fuel reliability and waste minimization to enhancing the accident-tolerance of Light Water Reactor (LWR) fuels. By definition, enhanced Accident Tolerant Fuels (ATFs) can tolerate loss of active cooling in the core for a considerably longer time period (depending on the LWR system and accident scenario) compared with the standard UO_2-zircaloy system currently used (Goldner, 2012). Furthermore, the ATF fuel/cladding system should maintain or improve the fuel performance during normal operations, operational transients, as well as design-basis (DB) and beyond design-basis (BDB) events Goldner, (2012).

Three potential approaches are proposed for the development of fuel/cladding systems that have enhanced accident tolerance (Ott et al., 2014; Zinkle et al., 2014).

1. Improve or replace the ceramic oxide fuel.
2. Modify current zircaloy cladding to achieve improved oxidation resistance, including application of coating layer.
3. Replace zircaloy cladding with an alternative oxidation-resistant high-performance cladding.

The evaluation of ATF should involve the assessment of its performance under normal operations and accident scenarios. One of the potential approaches that has been extensively explored is improving the oxidation resistance of the cladding.

* Corresponding author. Tel.: +1 217 979 7432.
E-mail addresses: xuwu2@illinois.edu (X. Wu), txk@illinois.edu (T. Kozlowski), jason.hales@inl.gov (J.D. Hales).

http://dx.doi.org/10.1016/j.anucene.2015.06.032
0306-4549/© 2015 Elsevier Ltd. All rights reserved.

Currently, the heat transfer coefficient between the zircaloy cladding exterior surface and the coolant is on the order of 1 W/(cm^2 K), under normal operating conditions (Terrani et al., 2014). However, under accident conditions, when the fuel rods are exposed to a slow flowing or stagnant steam, this parameter could decrease by four orders of magnitude, resulting in poor fuel cladding-to-coolant heat convection. Consequently, decay heat will drive up the fuel temperature, and a rapid exothermic zircaloy oxidation reaction will happen in the high-temperature steam environment, accompanied by significant hydrogen production. Zirconium cladding oxidation in high-temperature steam environments with poor heat transfer to the gaseous phase is characteristic of a self-catalytic process (at temperature higher than 1200 °C) (Terrani et al., 2014). The enthalpy production from oxidation reaction, along with the decay heat, will keep increasing the fuel temperature to the melting point. Therefore, cladding with improved oxidation resistance and less heat/hydrogen generation is expected to achieve larger margins of safety against severe accident scenarios.

Iron-based alloys, like standard commercial austenitic SS-310: Fe–25Cr–20Ni–2Mn, as well as Kanthal APMT (a commercial oxide dispersion strengthened [ODS] FeCrAl alloy) ferritic alloy: Fe–22C r–5Al–3Mo, were reexamined for their potential application as nuclear fuel cladding to replace zirconium alloys (Terrani et al., 2014). Two standard DB scenarios were investigated: LOCAs and Reactivity Insertion Accidents (RIAs). The magnitude of the parabolic oxidation rate constant for APMT and SS-310 were found to be roughly two to three orders of magnitude lower than what is observed for zirconium alloys.

Some other studies also identified a slow-growing alumina surface oxide formation during steam oxidation of APMT alloy (Cheng et al., 2012). This indicates a promising choice for nuclear fuel cladding under high temperature accident conditions. Post-quench ductility studies were conducted with zircaloy-4, stainless steel-(SS) 317, SS-347, and APMT alloy cladding samples at temperatures of 1200 °C, followed by cooling to 800 °C and then a water quench at room temperature to simulate the design basis Loss-of-Coolant Accident (LOCA) conditions and beyond (Yan et al., 2014). Among all the materials examined, the APMT sample showed the slowest oxidation rate.

Silicon Carbide (SiC) has also been proposed as a potential cladding material due to its low thermal neutron absorption cross-section, improved irradiation and oxidation resistance in air and steam up to temperatures of at least 1600 °C (Terrani et al., 2014). A known issue that limit the application of SiC in LWR fuel is the current lack of engineering familiarity in design and application. More engineering familiarity in the design and fabrication is required, as well as the test standards in nuclear applications. SiC is also known to be difficult to fabricate, and has low ductility compared with metallic cladding. These issues should be resolved before SiC finds application as nuclear fuel cladding. Nevertheless, its high thermal conductivity, excellent creep resistance, low thermal neutron absorption cross-section, and irradiation stability (minimal swelling) make it an excellent candidate material for future nuclear fuel/cladding systems.

TRACE and MELCOR were used to evaluate the impact of new candidate fuel/cladding materials (SS310, FeCrAl) on the reactor system under DB (RIA and LOCA) and BDB (short-term and long-term station blackout [STSBO, LTSBO]) accident conditions. The use of ATFs provides an increased time margin for accident response and mitigation measures. The additional time is approximately an hour to a few hours, and can serve as valuable response time for restoring core cooling and accident mitigation. The application of these ATFs also slowed hydrogen generation (Ott et al., 2014).

Even though much experimental research and system simulation under DB and BDB conditions has been done, no detailed evaluation of the impact of advanced cladding at normal operation conditions is available in the literature. In this paper, results for the fuel performance investigation and detailed simulation effort with the INL fuel performance analysis code BISON (Williamson et al., 2012) under normal operation conditions will be reported. Section 2 will discuss the composition, thermal–physical properties, other necessary material models such as thermal and irradiation creep, and oxidation behavior for FeCrAl. Sections 3 and 4 provide an overview of the neutronics analysis and fuel performance analysis with FeCrAl as alternate cladding material. Results and discussion are presented in Section 5, followed by conclusions in Section 6.

2. Thermal–physical properties of FeCrAl

2.1. Candidate materials

FeCrAl alloy and SS-310 represent the two major types of oxidation-resistant alloys at high temperature. The types of protective surface oxides or scales formed via selective oxidation are Al_2O_3 on APMT and Cr_2O_3 on SS-310 (Terrani et al., 2014). However, the material composition of a standard commercial austenitic 310 stainless steel (Fe–25Cr–20Ni–2Mn) has very high nickel concentration. The thermal neutron absorption cross-section of nickel is about twice that of iron. The parameter for iron is about 12–16 times higher than that of zirconium (Terrani et al., 2014). Therefore, SS-310 cladding is expected to have significant neutron penalty. Meanwhile, nickel could produce radioactive cobalt via the ^{58}Ni (n,p) ^{58}Co reaction. For these reasons, SS-310 is not considered as candidate cladding in this study.

Kanthal APMT FeCrAl alloy is one example of a class of alumina-forming ferritic alloys. The material composition used is 75% Fe, 20% Cr, and 5% Al. It includes ODS variants with increased creep resistance at high temperature (Terrani et al., 2014).

2.2. Cladding form

Possible forms for the application of the candidate cladding material are: (1) using it as monolithic cladding to replace zircaloy; (2) using it as a thin coating layer on the surface of zircaloy cladding.

A thin coating layer (100 micron thickness) is applied to the cladding surface. When exposed to steam during temperature excursions, this coating layer is expected to shift the M + O → MO reaction away from oxide growth to protect LWR fuel cladding (Heuser et al., 2013; Wu et al., 2014). However, recently researchers from ORNL identified some major drawbacks for this kind of cladding/coating system (Zinkle et al., 2014; Terrani et al., 2013, 2014), which include:

1. Careful matching of the thermal expansion coefficient for coating and cladding is necessary to minimize interfacial stresses and delamination during cycling (Zinkle et al., 2014).
2. Diametrical compression that results from reactor pressurization makes the application of coating layer problematic (generally requiring thin and highly adherent coatings) (Zinkle et al., 2014).
3. Different volumetric and microstructural evolution between the coating and underlying cladding under neutron irradiation can lead to coating spallation (Zinkle et al., 2014).
4. Once the fuel rod bursts, the inner zircaloy surface would be exposed to steam under accident conditions, resulting in rapid oxidation, heat generation and hydrogen production.

Therefore, high-temperature oxidation protection, especially in steam, is more readily and robustly accomplished by selective oxidation of one bulk component of the alloy than via coatings (Terrani et al., 2014).

5. Recently, it is reported SS-310 and FeCrAl could experience significant inter diffusion with zirconium (Terrani et al., 2013), which leads to an intermetallic layer with considerable thickness. Monolithic FeCrAl cladding is expected to perform better under high temperature steam environments in the absence of detrimental iron alloy–zirconium interactions.

Given the above considerations, FeCrAl should be applied as monolithic cladding rather than coating. However, one important disadvantage of FeCrAl application is in neutron penalty and consequent cycle length reduction, because iron has a thermal neutron absorption cross-section that is about 12–16 times higher than that of zirconium. There are several possible ways to enhance the end-of-cycle reactivity and thus increase the cycle length for nuclear fuel with monolithic iron based alloy cladding:

1. Increase the oxide fuel enrichment.
2. Minimize the cladding thickness. The advanced iron based alloys could enable fabrication of fuel cladding with thinner walls, because of their better strength, corrosion, and embrittlement properties.
3. Increase the mass of fuel inside the nuclear reactor. Since cladding thickness could be reduced, if the volume of fuel pins is maintained, the extra space gained could be filled with oxide fuels.

A most recent study (George et al., 2015) reported a good balance between option 2 and 3 by establishing an end-of-cycle (EOC) reactivity method to quantify the overall reactivity difference between different cladding models during an 18-month Pressurized Water Reactor (PWR) operating cycle. This article investigated austenitic type 310 and 304 stainless steels, ferritic Fe-20Cr-5Al (FeCrAl) and APMT™ alloys, and SiC-based materials as alternate cladding materials in a PWR, from the neutronics aspect. After detailed parametric study on the geometric conditions, it is reported that by using a thinner cladding of 350 μm and keeping a constant outer diameter, austenitic stainless steels require an increase of no more than 0.5 wt.% enriched U-235 to match fuel cycle length requirements, while the required increase for FeCrAl is 0.16%.

The design of FeCrAl cladding for fuel performance analysis in this paper is identical to the optimized design of FeCrAl cladding in the above mentioned study (George et al., 2015). The geometrical and compositional details of the neutronics model will be shown in Section 3, in which neutronics analysis using another code is presented to confirm the results from George et al. (2015).

2.3. Thermal–physical properties

Figs. 1–3 show various thermal–physical properties for zircaloy, UO_2 FeCrAl. Most of the properties are the same as those used in Ott et al. (2014), with a minor difference in UO_2 thermal conductivity. Here the Fink–Lucuta model defined in BISON theory manual (Hales et al., 2014) is used for UO_2 thermal conductivity.

Note that all the parameters shown in Figs. 1–3 are at zero burnup. In BISON, while the parameters for UO_2 and zircaloy have dependence on both temperature and either burnup or neutron flux and fluence, those for FeCrAl have only dependence on temperature. In addition, thermal conductivity values shown do not consider the effects of neutron irradiation. Tabulated material properties used in the paper are provided in the Appendix A.

For the specific heat capacity, the sharp spike for zircaloy is a result of a phase change (alpha to beta) from 1090 K to 1248 K. Similarly, the peak around 800 K for FeCrAl is due to a magnetic phase transition. The volumetric heat capacity and melting temperature could be found in Ott et al. (2014).

Normally it is expected fuel and cladding with higher volumetric heat capacity will demonstrate a slower transient thermal response. Lower cladding thermal conductivity would lead to higher initial fuel rod temperatures and higher initial stored energy when LOCA begins (Ott et al., 2014). However, slightly different results are found and will be presented in Section 5. The initial stored energy is not only dependent on thermal conductivity, but also on other material behaviors such as thermal and irradiation creep, as well as thermal expansion.

3. Model for neutronics analysis

As mentioned in Section 2.2, a recent study (Terrani et al., 2013; George et al., 2015) suggested an optimized design for FeCrAl cladding to replace current zircaloy cladding. Given the higher strength of iron-based alloys when compared with zirconium-based alloys, a reduced thickness of 350 μm (from 571.5 μm for zircaloy) for FeCrAl is suggested to meet lifetime requirements with only a slightly increased enrichment (0.16%), as well as maintaining cladding integrity during operations. For the cases studied in George et al. (2015), an outer rod diameter of 0.94996 cm is kept constant, therefore maintaining a pitch-to-rod ratio of 1.326 so that the thermal hydraulics in the PWR system would not be affected drastically if commercialized.

Before moving to fuel performance analysis, a neutronics study is carried out to confirm the results reported in George et al. (2015), in which a simple two-dimensional pin cell analyses were performed using SCALE/TRITON from SCALE 6.1.2. In this paper, FeCrAl cladding is used to replace zircaloy cladding in a PWR single assembly, which is based on the 17×17 Westinghouse design. Each assembly has 264 fuel pins and 25 guide tubes (here the central instrumentation tube is treated as a guide tube). The single assembly configuration is shown in Fig. 4.

A three-dimensional continuous-energy Monte Carlo reactor physics calculation code, Serpent, is used as the reactor neutronics code (Leppänen, 2007). To achieve sufficiently high calculation precision, 200 K neutrons per cycle are used with 100 inactive cycles and 1000 active cycles. This is sufficient to achieve eigenvalue statistical uncertainty of about 3 pcm.

At the top and bottom of the single assemblies, 30 cm of coolant is added as an axial reflector. Table 1 shows the neutronics model specifications. The same type of Zircaloy-4 material is used as cladding for the fuel pins and guide tubes. Table 1 shows the model specifications used in Serpent. All the dimensions, material compositions and operating conditions are same with that from George et al. (2015), except that here we use single assembly instead of a simple two-dimensional pin cell. Note that the specific power in megawatts per metric kilogram of uranium (MW/KgU) corresponds to the constant power of 18.0 KW/assembly modeled through the depletion cycle (George et al., 2015). The specific power density for fuel with FeCrAl clad is scaled down to keep a constant power per assembly.

4. Model for fuel performance analysis

INL's finite element-based nuclear fuel performance code BISON (Williamson et al., 2012) is used to model LWR nuclear fuel pin performance under normal operating conditions. BISON is built on MOOSE (Multi-physics Object Oriented Simulation Environment) framework (Gaston et al., 2009), which is a parallel computational framework designed for rapid production of new simulation tools.

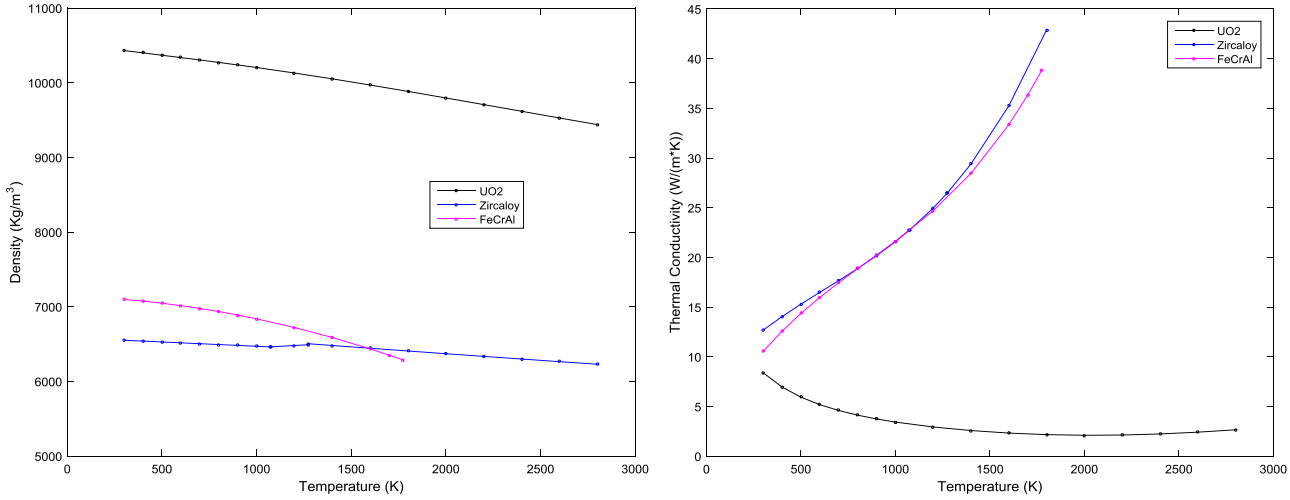

Fig. 1. Material density (left), thermal conductivity (right).

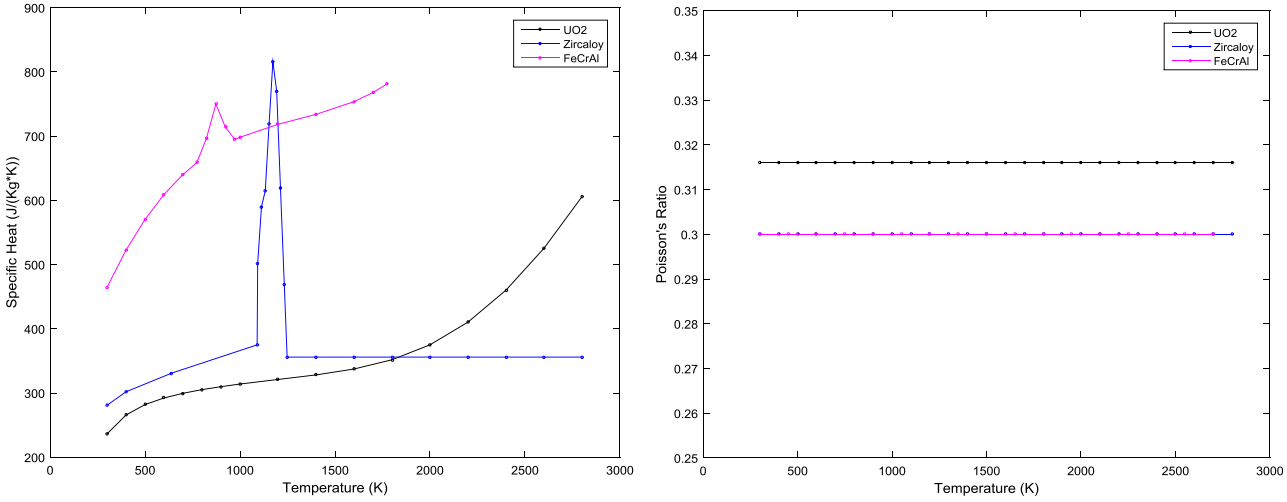

Fig. 2. Specific heat capacity (left), Poisson's ratio (right).

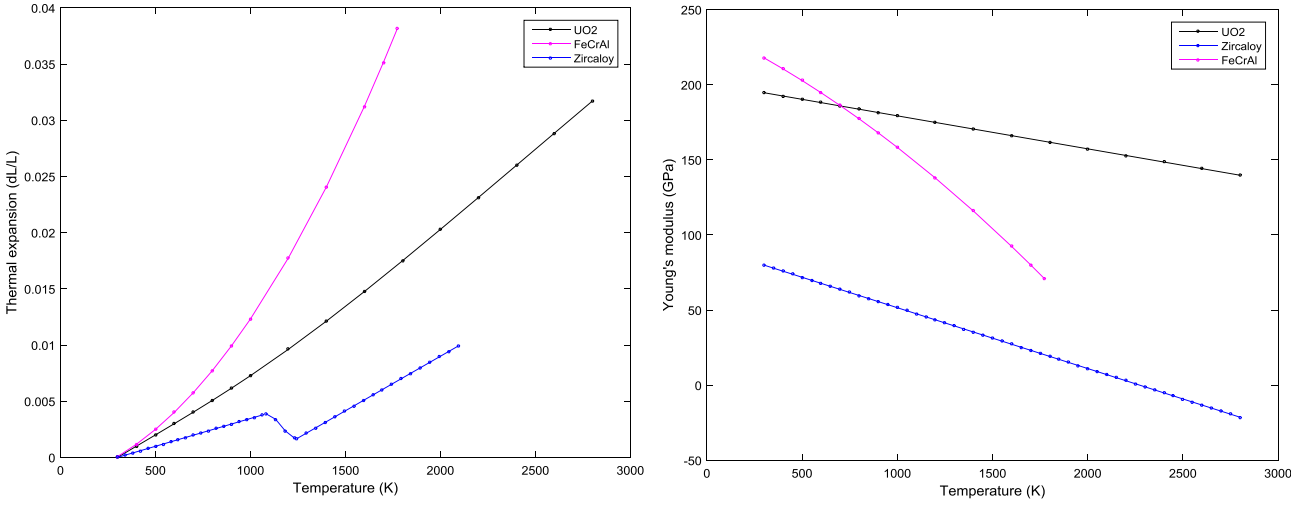

Fig. 3. Thermal expansion coefficient (left), Young's modulus (right).

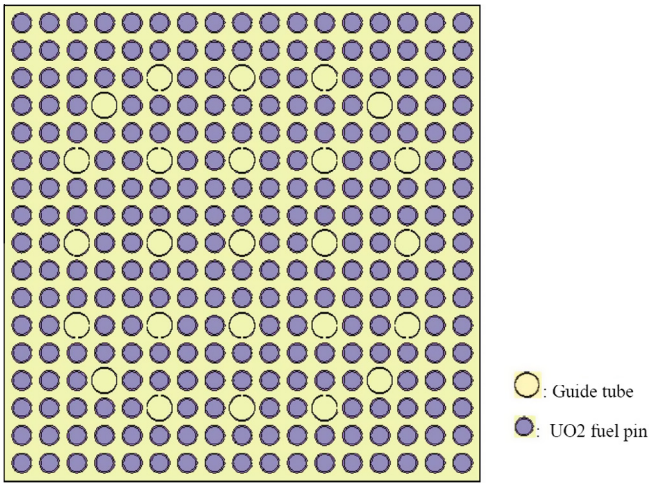

Fig. 4. UO_2 fuel assembly.

BISON solves the fully-coupled equations of thermo-mechanics and species diffusion, for either 1-D spherical, 2-D axisymmetric or 3-D geometries (Williamson et al., 2012, 2014; Hales et al., 2014). It incorporates a wide variety of material models for both fuel and zircaloy cladding. Temperature- and burnup-dependent thermal properties, as well as fission product swelling, densification, thermal and irradiation creep, fracture, and fission gas production and release are included for fuel models. For the cladding material, plasticity, irradiation growth, and thermal and irradiation creep models are implemented. Furthermore, BISON has models to simulate gas gap heat transfer, mechanical contact, and the evolution of the gap/plenum pressure with plenum volume, gas temperature, and fission gas addition. Detailed descriptions for all models and methods can be found in the BISON theory manual (Hales et al., 2014).

Table 1
Serpent model specifications.

Property	Value	
	Zircaloy-4 clad	FeCrAl clad
Assembly fuel height (cm)	365.76	
Clad composition:	Fe/Cr/Zr/Sn = 0.15/0.1/98.26/1.49 wt.%	Fe/Cr/Al = 75/20/5 wt.%
Fuel pellet radius (mm)	4.09575	4.31725
Gap thickness (μm)	82.55	
Cladding ID (mm)	4.1783	4.3998
Cladding thickness (μm)	571.5	350
Cladding OD (mm)	9.4996	
Pitch-to-rod-diameter ratio	1.326	
Cladding ID (mm)	5.624	
Cladding OD (mm)	6.032	
Number of guide tubes	25	
Fuel enrichment	4.90%	5.06%
Fuel density	10.47 g/cm^3	
Coolant density	0.7119 g/cm^3	
Cladding density	6.56 g/cm^3	7.10 g/cm^3
Specific power density (MW/KgU)	38.3300E-03	34.4798E-03
Simulated time (days)	1500.0	
Coolant temperature	580 K	
Fuel temperature	900 K	
Clad and gap temperature	600 K	
Boron concentration	630 ppm	
Neutron library	ENDF/B-VII	
Boundary conditions	Reflective	
Assembly design	Westinghouse 17 by 17 PWR fuel rod	

The LWR fuel pin model and mesh used in BISON are shown in Fig. 5 and Table 2. They include the model configuration, power history, and operational parameters. These parameters are based on the 2D-RZ 10-pellet rodlet example from the BISON workshop manual (Williamson et al., 2014). It is a well-established example and does not require excessive computational effort.

It is known from experiments the oxidation rate of FeCrAl is lower than that of zircaloy by at least two orders of magnitude (Ott et al., 2014). Also, oxidation under normal operation is not as important as that in accident conditions such as LOCA. Therefore, oxidation rates are set to 0 for both FeCrAl in the fuel performance analysis. Also, thermal or irradiation creep for FeCrAl is currently not available. For the fuel performance analysis in BISON, one case is executed with no creep for FeCrAl, while in another case, zircaloy creep model is used for FeCrAl. These two cases are used to bound the range of possible creep behavior of FeCrAl. This is a very optimistic estimate, since the creep for FeCrAl is assumed to be smaller than zircaloy in magnitude.

5. Results and discussion

5.1. Neutronics evaluation

As mentioned earlier, to enhance the reactivity and increase the cycle length when using FeCrAl as cladding, modified fuel rod geometries or increased enrichment in the fuel are necessary. By reducing the cladding thickness (from 571.5 μm to 350 μm), keep the fuel rod outer diameter gap thickness, filling extra space with fuel and slightly increase the fuel enrichment (from 4.90% to 5.06%), the multiplication factor k_{eff} evolution with effective full power days (EFPD) is shown in Fig. 6. Clearly the suggested design of FeCrAl cladding is able to maintain the required PWR cycle length. At the beginning of depletion, fuel with higher absorbing FeCrAl cladding shows a reduction in reactivity but a slight upsurge in reactivity near EOL. This phenomena is due to greater accumulation of plutonium near EOL and is demonstrated in Fig. 7.

Fig. 7 (left) shows the total Plutonium production over the depletion. It is indicated that despite differences in neutron absorption between zircaloy and FeCrAl, the total Plutonium production will not change significantly. Fig. 7 (right) shows radial distribution of Pu-239 in the pins at middle-of-life (MOL) and end-of-life (EOL), as Pu-239 is the largest contributor of fission reaction after U-235 in the fuel pin. Plutonium will accumulate on the periphery of fuel pellets as the depletion continues, because of spatial self-shielding of neutrons. The accumulation of additional fissile material will cause a sharp increase in fission near the edge of fuel pellets, known as the "Rim Effects". It is shown that fuel with FeCrAl cladding has a higher Pu-239 accumulation than fuel with zircaloy cladding and therefore a higher power, due to the harder neutron spectrum in the system causing more Pu-239 breeding.

Also, an economic assessment from George et al. (2015) shows that the increase in fuel pellet production costs for FeCrAl cladding is about 15%, which is the minimum among all the candidate materials considered, including austenitic type 310 and 304 stainless steels, ferritic Fe-20Cr-5Al (FeCrAl) and APMT™ alloys, and SiC-based materials. The increase in fuel pellet production costs is due to slightly increased U-235 enrichment and the additional UO_2 pellet volume enabled by decreasing clad thickness to nearly half to meet PWR lifetime requirements.

5.2. Fuel performance evaluation

The simulation time for the BISON models is 10^8 seconds, which is about 1160 days (3.2 years). A uniform convective boundary at

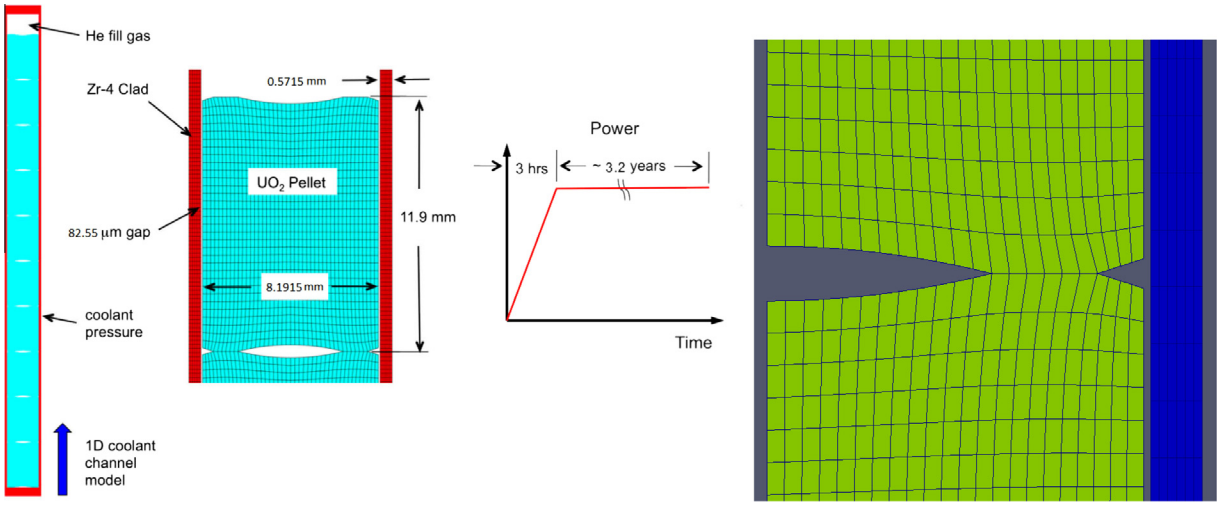

Fig. 5. Ten-pellet rodlet model (Williamson et al., 2014) and mesh.

Table 2
BISON model specifications.

Property	Value	
	Zircaloy-4 clad	FeCrAl clad
Active fuel rodlet height (cm)	11.90	
Fuel pellet radius (mm)	4.09575	4.31725
Gap thickness (μm)	82.55	
Cladding ID (mm)	4.1783	4.3998
Cladding thickness (μm)	571.5	350
Cladding OD (mm)	9.4996	
Pitch-to-rod-diameter ratio	1.326	
Fuel enrichment	4.90%	5.06%
Fuel theoretical density	96%	
Cladding density	6.56 g/cm^3	7.10 g/cm^3
Linear heat rate (W/cm)	250	
Simulated time (days)	1157.4	
Fast neutron flux (n/m^{2}s)	7.5×10^{17}	
Initial and inlet temperature	580 K	
Coolant pressure	15.5 MPa	
Coolant inlet mass flux	3800 kg/m^2-s	
Initial Helium pressure	2.0 MPa	

the clad outer wall is used to simulate heat transfer from the cladding surface to the coolant. The thermal-hydraulics model is simplified to a coolant channel, and details can be found in the BISON theory manual (Hales et al., 2014). The rodlet model uses discrete pellets.

Fig. 8 (left) shows fuel average burnup with respect to time for the three cases. Note that "FeCrAl cladding with creep" means zircaloy thermal and irradiation creep model is used for FeCrAl while keeping all the other properties for FeCrAl. Power history and axial power peaking factors are same for all three cases. Because fuel with FeCrAl cladding has a slightly higher enrichment, the burnup at the same time is lower than fuel with zircaloy cladding.

In Fig. 8 (right) the average fuel temperature evolution with burnup is presented. The average fuel temperature is defined as the average temperature of all the elements in the fuel region. To better interpret these results, a brief description of the nominal fuel temperature evolution in a PWR fuel rod is provided as the following stages:

1. At the beginning of depletion, fuel densification leads to the increase of the gap, thus the heat conduction gets worse, and fuel temperature increases.
2. Fuel swelling and clad creep are combined to reduce gap size, which causes fuel temperature to decrease.
3. Fission gas release begins at a burnup of around 10 MWd/kgU. The mixing of fission gas with helium in the plenum decreases thermal conductivity of gap, and fuel temperature increases.
4. This temperature increase is gradually reversed by continuing gap closure, until the gap is fully closed at approximately 36 MWd/kgU.
5. UO_2 thermal conductivity decreases with burnup; therefore, fuel temperature increases.

Note the time scale mentioned above is for a nominal PWR core modeled by BISON, not for the rodlet used here. From the above five steps, it is obvious fuel temperature is affected by many factors, such as fuel densification, fuel swelling, cladding thermal and irradiation creep, cladding thermal expansion, and cladding thermal conductivity. Special attention should be paid to Step 3 because fission gas release and fuel temperature increase form a positive feedback over a long burnup period. High fuel temperature will cause more fission gas release, and with the exacerbation of the gap conductance caused by fission gas, fuel temperature will increase. This positive feedback will be most pronounced while the gap is open.

Fig. 9 shows fission gas production and release over burnup. At each integration point, BISON computes the fission gas produced by a numerical time integration of the gas production rate, which is given as the product of fission rate and fractional yield of gas atoms per fission (with a value of 0.3017) (Williamson et al., 2012). Therefore, for all the cases, fission gas produced is the same as long as the power history is the same. So actually the three cases has the same fission gas production rate. But since the two cases with FeCrAl cladding have lower burnup at a given time, they have higher fission gas production at a given burnup compared with zircaloy cladding, as shown in Fig. 9 (left).

FeCrAl cladding with no creep has slightly higher fission gas release because the average fuel temperature is higher than the other cases, as indicated in Fig. 8 (right). To find out the reason for this phenomenon we need to look at Fig. 10, which shows the fuel rod internal volume and plenum pressure. Since there is not creep for this FeCrAl case, in stage 2 of the above temperature evolution, the gap size for this case will be larger, resulting in higher temperature. The subsequent fission gas release and fuel temperature increase form a positive feedback until it is reversed by continuing gap closure. Also, since cladding is not creeping inward,

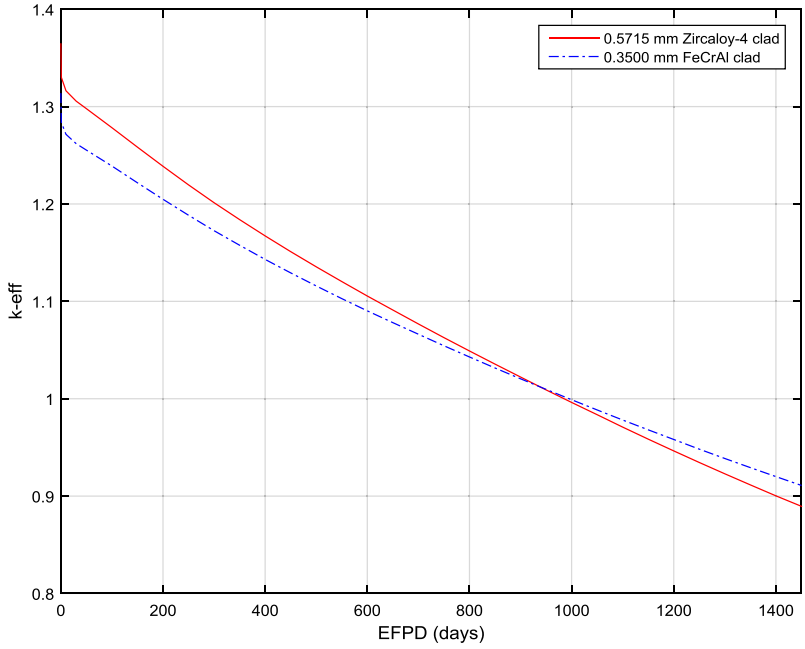

Fig. 6. Comparison of k_{eff} vs burnup for PWR single assembly.

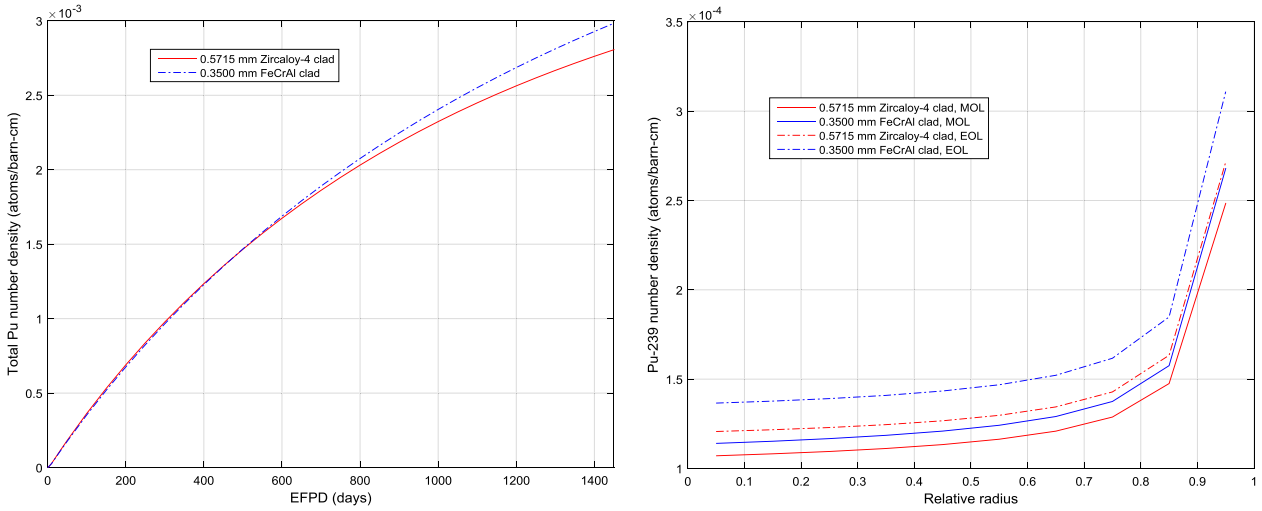

Fig. 7. Total Plutonium production (left) and Pu-239 radial distribution (right).

the interval volume is the highest and plenum pressure is the lowest among the three. Also, when we look at Zircaloy and FeCrAl with creep cases, FeCrAl has a similar thermal conductivity but a much higher specific heat capacity compared with zircaloy. This explains the lower average fuel temperature for FeCrAl cladding with creep.

Fig. 11 shows the axial temperature distribution and axial displacement of fuel centerline, at low burnup (10 MWd/KgU), medium burnup (30 MWd/KgU) and high burnup (50 MWd/KgU) for the three cases respectively. With the increase of burnup, the difference in axial temperatures of the fuel centerline decreases. Furthermore, the axial temperature profile is flattened for FeCrAl cladding with no creep, also the axial displacement is lowest at medium to high burnup for this case.

Fig. 12 shows the radial temperature profile and radial displacement of the horizontal line at the center of the 5th pellet from the bottom (which is close to the center of the fuel rod), at low, medium and high burnup steps. Similarly, the difference in axial temperature profiles for the three cases decreases with the increase of burnup, but generally temperature profiles for zircaloy case fall between the two FeCrAl cases. In Fig. 12 (right), the left part (before the sudden drop) indicates the radial displacement in the fuel region, and the right part (after the sudden drop) means radial displacement for the cladding region. The cladding region clearly demonstrates that FeCrAl with creep case and zircaloy case are creeping inward, while FeCrAl with no creep case only has very small radial displacement at high burnup. The radial displacement in the fuel region is due to thermal expansion and swelling of UO_2.

Fig. 13 shows the radial power factor and radial Pu-239 distribution of the horizontal line at the center of the 5th pellet from the bottom, at low, medium and high burnup steps. The "Rim Effect" needs to be captured in order to calculate the heat generation and temperature distribution in the pellet accurately. BISON uses the TUBRNP model of Lassmann et al. (1994). From Fig. 13,

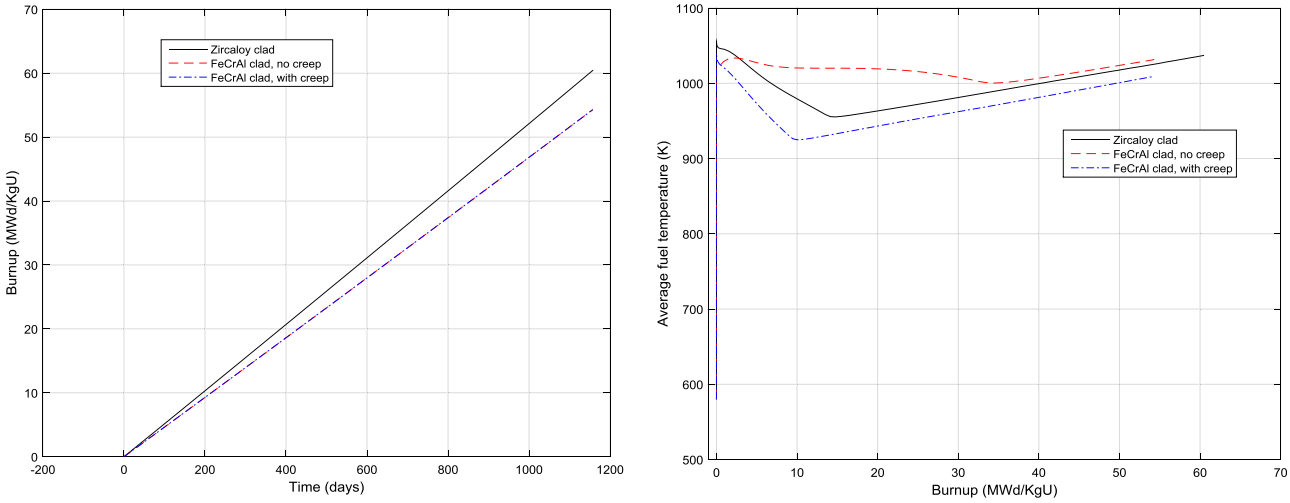

Fig. 8. (Left) Burnup vs time, (right) average fuel temperature.

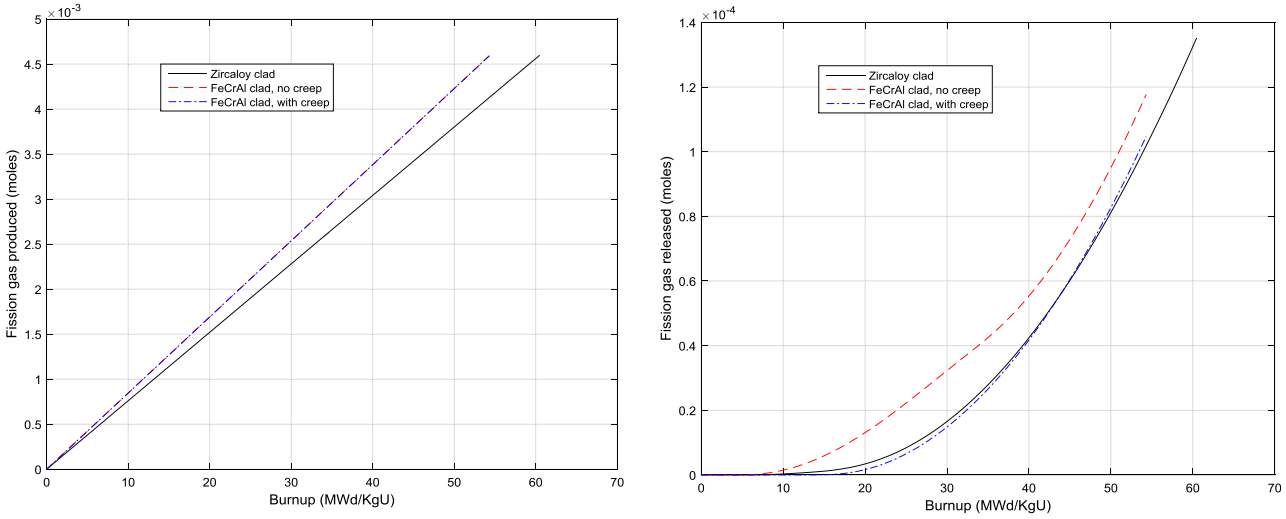

Fig. 9. (Left) Fission gas produced, (right) fission gas released.

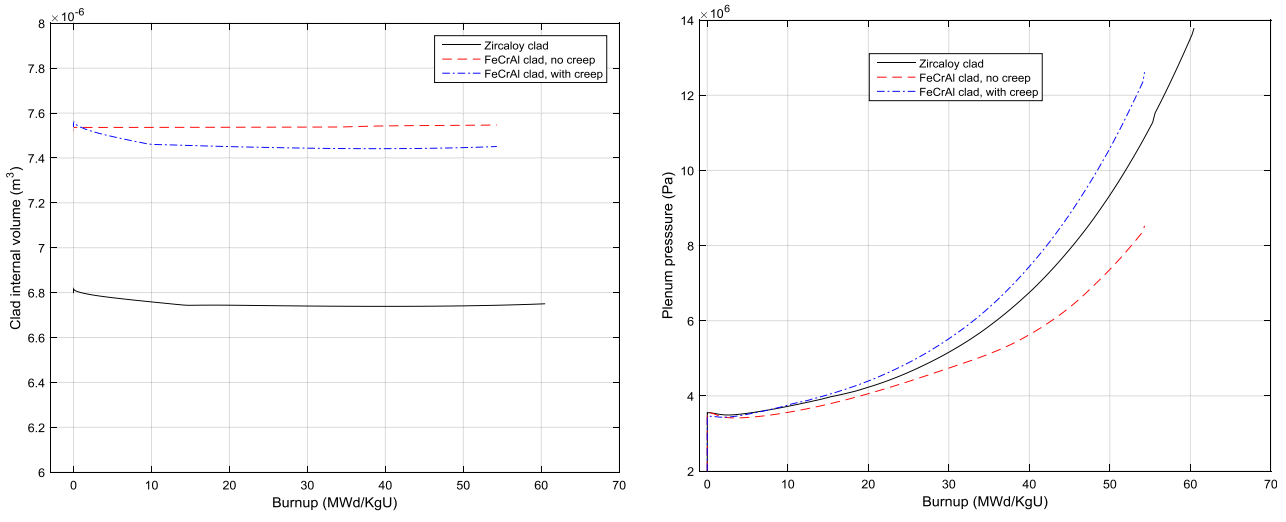

Fig. 10. (Left) Internal volume, (right) plenum pressure.

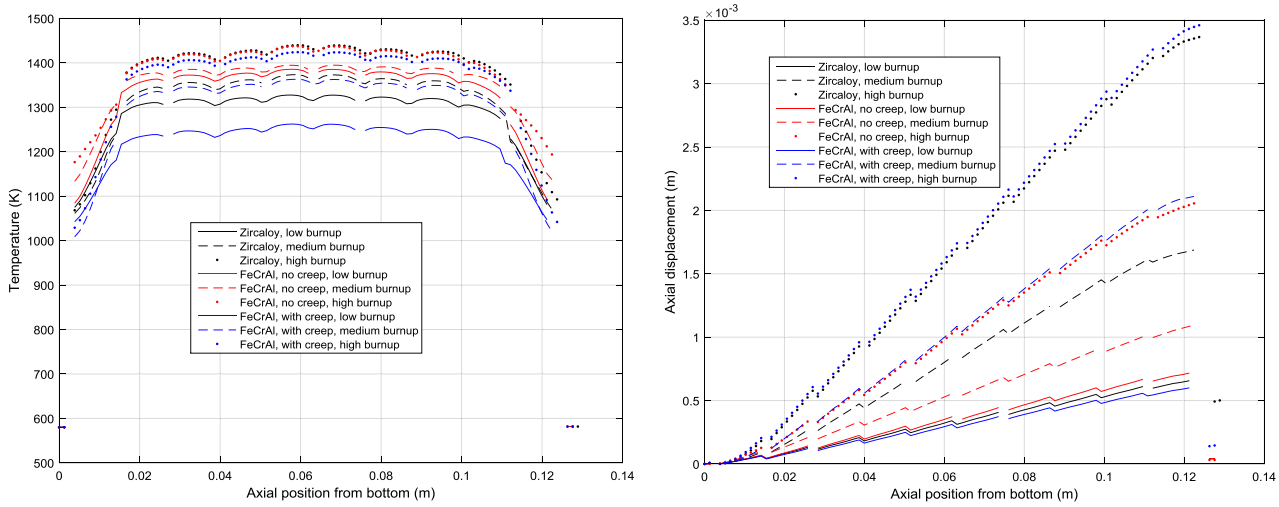

Fig. 11. (Left) Temperature distribution over the fuel centerline at different burnup, (right) axial displacement over the fuel centerline at different burnup.

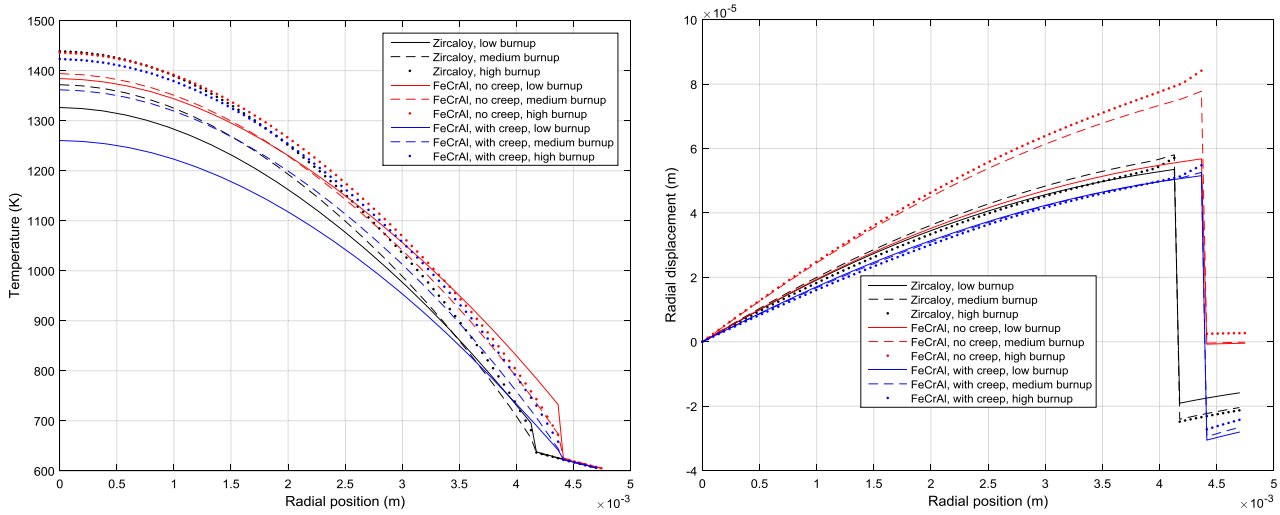

Fig. 12. Plot over the horizontal center line of the fifth fuel pellet from bottom at different burnup, (left): radial temperature distribution, (right): radial displacement.

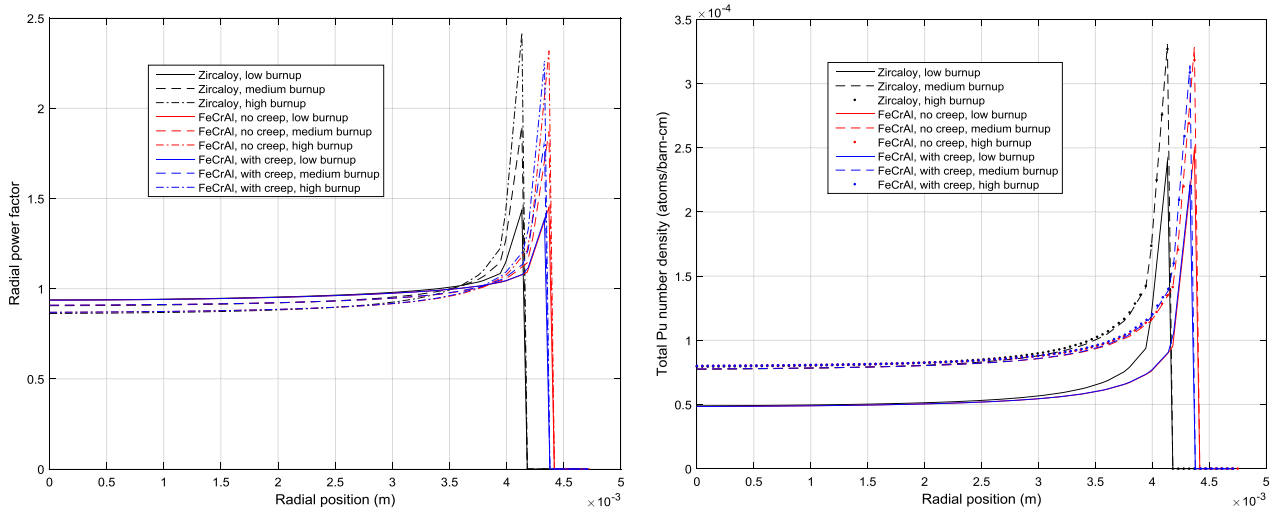

Fig. 13. Plot over the horizontal center line of the fifth fuel pellet from bottom at different burnup, (left): radial power factor, (right) radial Pu-239 distribution.

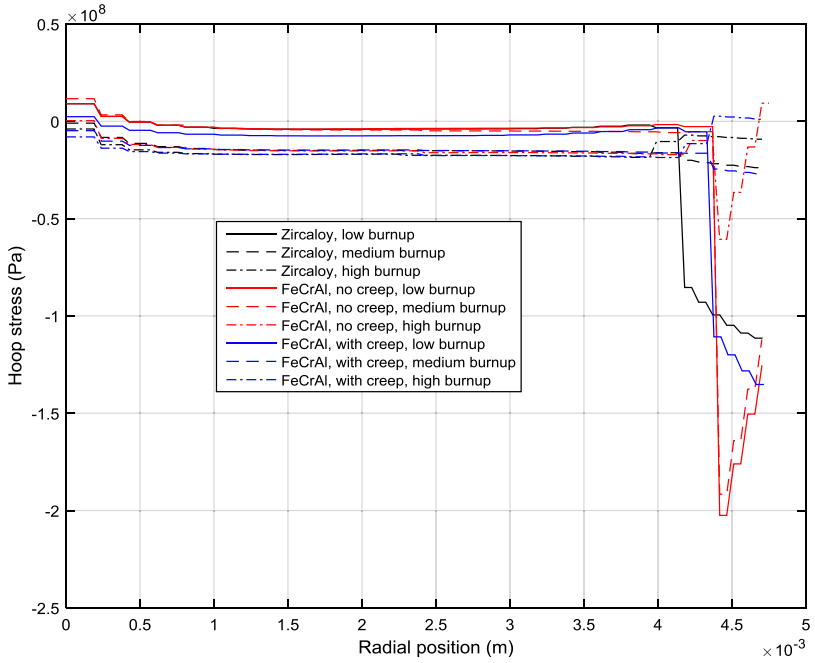

Fig. 14. Hoop stress over the horizontal center line of the fifth fuel pellet from bottom at different burnup.

there is no considerable difference in the radial power factors and Pu-239 accumulation. The difference in radial positions is due to the different radial geometries between fuel rods with Zircaloy and FeCrAl cladding.

Fig. 14 demonstrates the distribution of hoop stress of the same horizontal line at different burnup steps. Maximum cladding hoop stress and maximum fuel rod centerline temperature are primary parameters to identify the regions for potential failure. It is noticed that hoop stress is largest at low burnup, while the coolant pressure is the primary contributor to the stress state in the cladding. The figure shows that FeCrAl cladding with no creep has much larger hoop stress at each burnup (especially for low to medium burnup). The reason is related to the creep behavior of the cladding. Cladding creeping inward will cause the gap size to decrease which causes earlier contact of fuel pellet and cladding (as shown in Fig. 15). Since we know that there will be thermal and irradiation creep for FeCrAl, the hoop stress will not be as large as shown by the red lines in Fig. 14. However, special attention should be paid to FeCrAl cladding to make sure it will not fail because of hoop stress at low to medium burnup.

Fig. 15 presents the gap sizes behavior of two nodes on the pellet surface. Point 1 is at the height of 0.012 m (around center of the

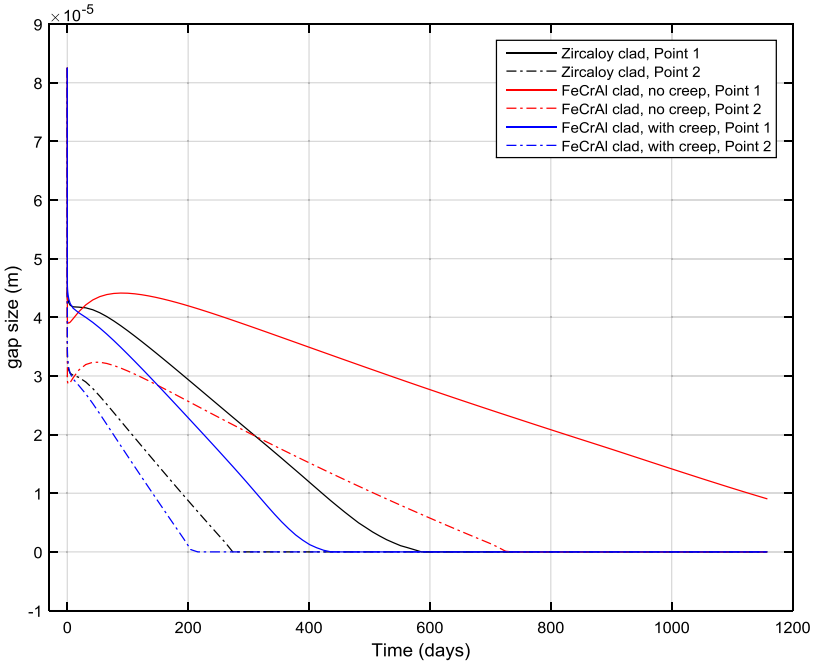

Fig. 15. Plot of gap sizes for two nodes on fuel pellet surface, point 1 is at the height of 0.012 m, point 2 is at the height of 0.07 m.

Table 3
Comparison of effective multiplication factor k_{eff} for PWR single assembly with various cladding material combinations.

Temperature	Density	Thermal Conductivity	Specific Heat	Thermal Expansion	Poisson's Ratio	Young's Modulus
K	kg/m^3	$W/(m \cdot K)$	$J/(kg \cdot K)$			GPa

first pellet from bottom), and point 2 is at height of 0.07 m (center of the fifth pellet from bottom). It is summarized that:

1. At the beginning of simulation (power ramp over 3 h), gap width rapidly decreased from 0.08 mm to 0.03–0.04 mm due to fuel densification.
2. Gap will continue to decrease as a combination of fuel densification, fuel swelling, fuel thermal expansion and clad creep. But within the first 50 days of depletion, FeCrAl case with no creep undergo a slight gap increase because there is no cladding creep inward to counteract the decrease in gap size.
3. FeCrAl clad with no creep shows that gap closure can be delayed greatly, by more than 400 days. This means Pellet-Cladding Mechanical Interaction (PCMI) is significantly delayed.
4. Gap closure occurs at very different time for different location in the fuel pins.

5.3. Comparison of zircaloy and FeCrAl

The excellent performance of FeCrAl alloy has already been validated in experimental investigation (Zinkle et al., 2014; Terrani et al., 2013, 2014; Cheng et al., 2012; Yan et al., 2014) and system simulation using TRACE and MELCOR (Ott et al., 2014). Based on the results from Serpent and BISON presented in Sections 5.1 and 5.2, an evaluation of FeCrAl based on neutronics and fuel performance analysis will be discussed here:

1. The utilization of FeCrAl to replace current zircaloy cladding requires a reduction in cladding thickness and a slight increase in fuel enrichment, in order to overcome the neutron penalty and resulting decrease in PWR cycle length.
2. The optimized design proposed in George et al. (2015) is confirmed with a PWR single assembly neutronics analysis with Serpent code. This design includes keeping the fuel rod outer radius and gap size, reducing cladding thickness from 571.5 μm to 350 μm, and increasing fuel enrichment from 4.9% to 5.06%. The PWR cycle length will be preserved in this way, but the fuel pellet production costs for FeCrAl cladding will increase by about 15%.
3. It is shown that higher thermal conductivity does not necessarily lead to lower fuel temperature and lower initial stored energy upon LOCA, unless the gap is closed. Creep, either caused by heat or irradiation, is proven to play an important role in the evolution of fuel temperatures. Creep of cladding could reduce gap size and decrease fuel temperature over the burnup.
4. However, irradiation creep of zirconium is known to be a primary contributor to geometrical changes in fuel rods, which may be not desirable. For example, in a PWR reactor, permanent deformation of the fuel assemblies (like bowing) could lead to serious issues such as control rod drop failure or increased drop time, exacerbated local cooling, etc.
5. Other impacts of using FeCrAl include reduced plenum pressure, flattened axial power profile, as well as greatly delayed gap closure time.

6. Conclusions

Neutronics and fuel performance analysis is done for enhanced accident tolerance fuel, with the Monte Carlo reactor physics code Serpent and INL's fuel performance code BISON. The purpose is to evaluate the most promising candidate material FeCrAl, which has excellent oxidation resistance, as fuel cladding under normal operational conditions.

Table 4
Dependence of Zircaloy density and specific heat capacity on temperature for Zircaloy.

Temperature	Density	Temperature	Specific heat
300	6551.38	300	281
400	6539.685	400	302
500	6528.032	640	331
600	6516.42	1090	375
700	6504.85	1093	502
800	6493.32	1113	590
900	6481.831	1133	615
1000	6470.383	1153	719
1073.15	6462.035	1173	816
1074	6462.3	1193	770
1200	6480.342	1213	619
1273.15	6490.862	1233	469
1274	6504.407	1248	356
1400	6480.815	1400	356
1600	6443.717	1600	356
1800	6407.041	1800	356

Detailed discussion of whether to apply FeCrAl as monolithic cladding or coating on zircaloy cladding is provided in Section 2.2. Due to several major disadvantages of FeCrAl coating, such as difficulty in fabrication, diametrical compression from reactor pressurization, coating spallation and inter-diffusion with zirconium, the monolithic FeCrAl cladding design is chosen. However, a substantial neutron penalty is expected when FeCrAl is used as cladding for current oxide fuel. To compensate for the drop in reactivity, several approaches are discussed in Section 2.2, including: (1) increasing the oxide fuel enrichment; (2) minimizing the cladding thickness to reduce the neutron penalty; and (3) reducing the cladding thickness and filling the extra volume with oxide fuel.

This paper adopted the optimized FeCrAl cladding design from a detailed parametric study reported in George et al. (2015), which suggests reducing the cladding thickness and slightly increasing the fuel enrichment. A neutronics analysis is done that implementing this FeCrAl cladding design in a PWR single assembly. The results confirms that the PWR cycle length requirements will be matched, with a slight increase in total plutonium production. However, it is also reported in George et al. (2015) that this optimized design will cause a 15% increase in fuel pellet production cost.

Fuel performance analysis under normal operation conditions with INL code BISON is carried out to investigate the effects with this FeCrAl cladding design. The results from fuel performance analysis demonstrate that the application of FeCrAl cladding could improve performance. For example, the axial temperature profile is flattened. The gap closure is significantly delayed, which means the pellet-cladding mechanical interaction is greatly delayed. The disadvantages for FeCrAl cladding are that: (1) fission gas release is increased; and (2) fuel temperature is increased, but the increase is less than 50 K even at high burnup.

Based on the above discussion, applying FeCrAl as monolithic cladding to replace current zircaloy cladding will help avoid the major disadvantages for FeCrAl coating design. The better strength, corrosion, and embrittlement properties of FeCrAl enable the fabrication of FeCrAl cladding with thinner walls. With the optimized design suggested in George et al. (2015), FeCrAl cladding proves to be a good alternate for zircaloy cladding, given the advantages and insignificant disadvantages shown by fuel performance analysis.

Appendix A

The material properties for UO_2, zircaloy and FeCrAl used in this paper are provided here. As is mentioned in Section 2.3, most of the properties are the same with an earlier article (Ott et al., 2014), with minor differences in UO_2 thermal conductivity from BISON theory manual (Hales et al., 2014). The symbols and units for the thermal–mechanical properties are summarized in Table 3.

A.1. UO_2

$$\rho_{UO_2} = 0.95 \times 10.98 \times \left[1.0 - 3.0 \times \left(\frac{\Delta L}{L(300\,\mathrm{K})}\right)_{UO_2}\right] \quad 300\,\mathrm{K} \leqslant T \leqslant 2800\,\mathrm{K}$$

$$\left(\frac{\Delta L}{L(300\,\mathrm{K})}\right)_{Zry} = \begin{cases} 4.95 \times 10^{-6} \cdot T - 1.485 \times 10^{-3} & 300\,\mathrm{K} \leqslant T \leqslant 1083\,\mathrm{K} \\ 2.77763 \times 10^{-3} + 1.09822 \times 10^{-3} \cdot \cos\left(\pi \cdot \frac{T-1083}{161}\right) & 1083K \leqslant T \leqslant 1244\,\mathrm{K} \\ 9.7 \times 10^{-6} \cdot T - 1.04 \times 10^{-2} & 1244K \leqslant T \leqslant 2098\,\mathrm{K} \end{cases}$$

$$(c_p)_{UO_2} = 296.7 \times \left(\frac{535.285}{T}\right)^2 \times e^{\frac{535.285}{T}} \Big/ \left(e^{\frac{535.285}{T}} - 1.0\right)^2 + 2.43 \times 10^{-2} \cdot T + (1.65869 \times 10^{12}) * e^{(-1.8967 \times 10^4/T)}/T^2 \quad 300\,\mathrm{K} \leqslant T \leqslant 2800\,\mathrm{K}$$

$$\left(\frac{\Delta L}{L(300\,\mathrm{K})}\right)_{UO_2} = -3.0 \times 10^{-3} + 1.0 \times 10^{-5} \cdot T + 4.0 \times 10^{-2} \cdot e^{5000.0/T} \quad 300\,\mathrm{K} \leqslant T \leqslant 2800\,\mathrm{K}$$

$$\nu_{UO_2} = 0.316$$

$$E_{UO_2} = 201.2842 \times (1.0 - 1.0915 \times 10^{-4} \cdot T) \quad 300\,\mathrm{K} \leqslant T \leqslant 2800\,\mathrm{K}$$

The thermal conductivity for UO_2 is a complicated correlation called Fink-Lucuta model defined in Hales et al. (2014):

$$k_{UO_2} = k \cdot f_d \cdot f_p \cdot f_{por} \cdot f_r \quad 298\,\mathrm{K} \leqslant T \leqslant 3120\,\mathrm{K}$$

where:

$T_n = T/1000$, T is the temperature in K.

$k = \left(\frac{1}{7.5408 + 17.692 \cdot T_n + 3.6142 \cdot T_n^2} + \frac{6400}{T_n^{2.5}} \exp\left(-\frac{16.35}{T_n}\right)\right) \cdot \left(\frac{1}{1 - (2.6 - 0.5 \cdot T_n) \cdot 0.05}\right)$, which is the thermal conductivity at 100% theoretical density.

$f_d = \left(\frac{1.09}{bu^{3.265}} + 0.0643 \cdot \sqrt{\frac{T}{bu}}\right) \cdot \arctan\left(\frac{1.0}{\frac{1.09}{bu^{3.265}} + 0.0643 \cdot \sqrt{\frac{T}{bu}}}\right)$, which is the dissolved fission products correction, bu is the burnup in at.%.

$f_p = 1.0 + \left(\frac{0.019 \cdot bu}{3.0 - 0.019 \cdot bu}\right) \cdot \left(\frac{1.0}{1.0 + \exp\left(\frac{-(T-1200)}{100}\right)}\right)$, which is the precipitated fission products correction.

$f_{por} = \left(\frac{1.0 - p}{1.0 + 0.5 \cdot p}\right)$, which is the porosity correction, p is the porosity.

$f_r = 1.0 - \frac{0.2}{1.0 + \exp\left(\frac{T-900}{80}\right)}$, which is the radiation damage correction.

A.2. Zircaloy

$$k_{Zry} = 7.511 + 2.088 \times 10^{-2} \cdot T - 1.450 \times 10^{-5} \cdot T^2 + 7.668 \times 10^{-9} \cdot T^3 \quad 300\,\mathrm{K} \leqslant T \leqslant 1800\,\mathrm{K}$$

$$\nu_{Zry} = 0.3$$

$$E_{Zry} = 92.1 - 4.05 \times 10^{-2} \cdot T \quad 300\,\mathrm{K} \leqslant T \leqslant 1800\,\mathrm{K}$$

The material density and specific heat capacity for Zircaloy is provided in Table 4.

A.3. FeCrAl

$$\rho_{FeCrAl} = 7.10 - 21.30 \times (-1.938 \times 10^{-3} + 3.450 \times 10^{-6} \cdot T + 1.080 \times 10^{-8} \cdot T^2) \quad 300\,\mathrm{K} \leqslant T \leqslant 1773\,\mathrm{K}$$

$$k_{FeCrAl} = 2.53282 + 3.2532 \times 10^{-2} \cdot T - 2.2 \times 10^{-5} \cdot T^2 + 8.5645 \times 10^{-9} \cdot T^3 \quad 300\,\mathrm{K} \leqslant T \leqslant 1773\,\mathrm{K}$$

$$(c_p)_{FeCrAl} = \begin{cases} 220.6822 + 1.012945 \cdot T - 7.19279 \times 10^{-4} \cdot T^2 + 1.84 \times 10^{-7} \cdot T^3 & 300\,\mathrm{K} \leqslant T \leqslant 773\,\mathrm{K} \\ 2145.283 - 4.43229 \cdot T + 3.246312 \times 10^{-3} \cdot T^2 & 773\,\mathrm{K} \leqslant T \leqslant 873\,\mathrm{K} \\ 4083.095 - 6.74839 \cdot T + 3.356712 \times 10^{-3} \cdot T^2 & 873\,\mathrm{K} \leqslant T \leqslant 973\,\mathrm{K} \\ 220.6822 + 1.012945 \cdot T - 7.19279 \times 10^{-4} \cdot T^2 + 1.84 \times 10^{-7} \cdot T^3 & 973\,\mathrm{K} \leqslant T \leqslant 1773\,\mathrm{K} \end{cases}$$

$$\left(\frac{\Delta L}{L(293\ \mathrm{K})}\right)_{\mathrm{FeCrAl}} = -1.938\times10^{-3} + 3.450\times10^{-6}\cdot T + 1.080\times10^{-8}\cdot T^2 \quad 300\ \mathrm{K} \leqslant T \leqslant 1773\ \mathrm{K}$$

$$\nu_{\mathrm{FeCrAl}} = 0.3$$

$$E_{\mathrm{FeCrAl}} = 237.7808 - 6.041\times10^{-2}\cdot T - 1.9\times10^{-5}\cdot T^2 \quad 300\ \mathrm{K} \leqslant T \leqslant 1773\ \mathrm{K}$$

References

Cheng, T., Keiser, J., Brady, M., Terrani, K., Pint, B., 2012. Oxidation of fuel cladding candidate materials in steam environments at high temperature and pressure. J. Nucl. Mater. 427 (1), 396–400.

Gaston, D., Newman, C., Hansen, G., Lebrun-Grandie, D., 2009. MOOSE: a parallel computational framework for coupled systems of nonlinear equations. Nucl. Eng. Des. 239 (10), 1768–1778.

George, N.M., Terrani, K., Powers, J., Worrall, A., Maldonado, I., 2015. Neutronic analysis of candidate accident-tolerant cladding concepts in pressurized water reactors. Ann. Nucl. Energy 75, 703–712.

Goldner, F., 2012. Development Strategy for Advanced LWR Fuels with Enhanced Accident Tolerance. In: Enhanced Accident Tolerant LWR Fuels National Metrics Workshop, Germantown, Maryland, October 2012.

Hales, J. D., Novascone, S., Pastore, G. Perez, D., Spencer, B., Williamson, R., 2014. BISON Theory Manual: The Equations behind Nuclear Fuel Analysis, Fuels Modeling & Simulation Department, Idaho National Laboratory, Idaho Falls, Idaho, June 2014.

Heuser, B.J., Kozlowski, T., Wu, X., 2013. Engineered Zircaloy Cladding Modifications for Improved Accident Tolerance of LWR Fuel: A Summary. In: Proc. of the 2013 LWR Fuel Performance Meeting/TopFuel, Charlotte, North Carolina, USA, September 15–19, 2013.

Lassmann, K., O'Carroll, C., van de Laar, J., Walker, C.T., 1994. The radial distribution of plutonium in high burnup UO2 fuels. J. Nucl. Mater. 208, 223–231.

Leppänen, J., 2007, Development of a New Monte Carlo Reactor Physics Code (Ph.D. Thesis). VTT Technical Research Centre of Finland, Espoo, Finland.

Ott, L.J., Robb, K., Wang, D., 2014. Preliminary assessment of accident-tolerant fuels on LWR performance during normal operation and under DB and BDB accident condition. J. Nucl. Mater. 448 (1), 520–533.

Terrani, K.A., Parish, C., Shin, D., Pint, B., 2013. Protection of zirconium by alumina- and chromia-forming iron alloys under high-temperature steam exposure. J. Nucl. Mater. 438 (1), 64–71.

Terrani, K.A., Zinkle, S., Snead, L., 2014. Advanced oxidation-resistant iron-based alloys for LWR fuel cladding. J. Nucl. Mater. 448 (1), 420–435.

Terrani, K.A., Pint, B.A., Parish, C.M., Silva, C.M., Snead, L.L., katoh, Y., 2014. Silicon carbide oxidation in steam up to 2 MPa. J. Am. Ceram. Soc. 97, 2331–2352.

Williamson, R.L., Hales, J., Novascone, S., Tonks, M., Gaston, D., Permann, C., Andrs, D., Martineau, R., 2012. Multidimensional multiphysics simulation of nuclear fuel behavior. J. Nucl. Mater. 423 (1), 149–163.

Williamson, R.L., et al., 2014. Implicit, parallel, fully-coupled nuclear fuel performance analysis. In: Fuels Modeling & Simulation Department BISON Workshop, Idaho National Laboratory, Idaho Falls, Idaho, June 2014.

Wu, X., Kozlowski, T., Heuser, B., 2014. Neutronics Analysis of Improved Accident Tolerance of LWR Fuel by Modifying Zircaloy Cladding of Fuel Pins. In: Proceedings of ICAPP-2014, Charlotte, USA, April 6–9, 2014.

Yan, Y., Keiser, J., Terrani, K., Bell, G., Snead, L., 2014. Post-quench ductility evaluation of Zircaloy-4 and select iron alloys under design basis and extended LOCA conditions. J. Nucl. Mater. 448 (1), 436–440.

Zinkle, S.J., Terrani, K., Gehin, J., Ott, L., Snead, L., 2014. Accident tolerant fuels for LWRs: a perspective. J. Nucl. Mater. 448 (1), 374–379.